RESEARCH REVIEW JOURNALS
Volume-04
Issue-03
March-2019

ISSN: 2455-3085 (Online)
RESEARCH REVIEW International Journal of Multidisciplinary
www.rrjournals.com[UGC Listed Journal]

A Study of Preoccupation of Nickel Nanoparticles Physical Characteristics

[1]Sweety and [2]Dr.Vipin Kumar

[1]Research Scholar, OPJS University, Churu, Rajasthan
[2]Professor, OPJS University, Churu, Rajasthan

ARTICLE DETAILS

Article History
Published Online: 13 March2019

Keywords
Preoccupation, Nickel, Nanoparticles Physical, Nano-Grids, processes, nanoparticles.

ABSTRACT

The design of Nano-Grids was provisionally understood in two ways. Next, a surfactant head (P or TOP) binds to a Ni particle surface while organic tail joins a new surfactant tail to bind particles at a fixed distance. With the increase in the number of such processes, Nano grids are formed to reduce overall superficial energy. Second, the Zeta potentials indicate that FTIR and XPS data can attract the anions of the surrounding nanoparticles until they sense the presence of other ion pairs of the dissociated surface molecules or impurities attached to nanoparticles that lead to repulsion.The content of one of the favorite surfactants or stabilizer among researchers, namely oleylamine (OA), TOP or tryphenylphosphine (TPS), varying one of them, or using just one surfactant separately, nickel nanoparticles by thermal decomposition of nickel acetylacetonate. Data was used to describe the formation of nano-latte to potential non-ionic trioctyl phosphine generating anion cation pairs from potential zeta studies. This contributes to their surface loading and subsequently changes of the zeta potential. Of note, in comparison with broader ones for randomly agglomerated particles, the narrowest zeta potentials (z) base widths were observed for samples possessing an autoassemblednanostrip. The characteristic exponential quantum-sized effect attributed to Ni nanoparticles is an exceptional discovery pending from its prediction and is exemplary for the almost theoretical one particle existence of the hot-capacity metal nanoparticles. The natural Nano-Lattic formulation approach, its physical properties, and insight into its design state pave the way for the creation and discovery of both new groups of natural Nano-Lattic products for basic studies.

1. Introduction

The exponentially decaying heat capacity CP at low temperature (T→0) of metal nanoparticles for equal level spacing (δ) due to quantum size effect (QSE) has not yet been observed experimentally except their reduction or enhancement, compared to their bulk counterparts. This null observance, in contrast to quantum size effects observed in facsimile ways in other various physical parameters is attributed to the high sensitivities to uncontrollable influences of their matrices or environment and to natural difficulties in obtaining ideally monodispersed metal nanoparticles. The difficulty in the experimental observation of exponentially decaying heat capacity of metal nanoparticles (MNPs) has been believed to be due to the simple theoretical assumptions that cannot meet the real experimentally challenging environments. They include (i) a single metal particle not able to meet the thermodynamic nature of heat capacity (ii) size effect limitation d ≥ 10 nm with T < 0.1 K to avoid surface effects(iii) matrix disturbance on metal particles' propertiesand (iv) smoothening of level spacings in an ensemble of practically monodispersed particles. The typical samples used have been compacted gas-/ thermally-evaporated Pdnanoparticles (NPs), polyol-method13 and thermal decomposition prepared Ni NPs, in which at least some surface oxidation naturally occurs in addition to the interactions with surfactants/ matrices.

Stewart, for example, reported a reduced heat capacity of Pt NPs embedded in SiO2 at low temperatures and argued it to be a manifestation of QSE. However, majority of enhancement was attributed to the matrix, say SiO2 since Pt and SiO2 were cosputtered. The problem was that he subtracted the bulk values of heat capacity of Pt and vitreous silica from nanoparticle data with the disadvantage of large error involved especially from the sputtered SiO2 by taking the values of vitreous silica directly. Schmidt et al. reported a negative micro canonical heat capacity near the solid to liquid transition on cluster of 147 sodium atoms produced in a gas aggregation source. Volokitin et al. based on the presence of spurious magnetic impurities especially in Pd, on the other hand reported the odd-even electron spin states predicted for QSE with the significant influence of the magnetic field on the magnetic susceptibility and specific heat below 0.2 K of shellularPd clusters but not in colloidal Pd. Moreover, exponentially decaying CP was ruled out with no quantum jumps. In contrast, in all the other cases such as Al, V, In, Sn, Pt and Pb, enhanced CP only have been reported and the same have been attributed either to QSEs of the vibrational spectrum of nanoparticles, or an increased electronic heat capacity most likely associated with the surface states of the nanoparticles. Thus, the environment of each system of MNPs in earlier works finally appear to turn out to be contrary to that required theoretically on quantum size effect of exponentially decaying CP, leading to null result. In contrast, we show here the definitively exponentially decaying heat capacity, below 45.2 K, associated with quantum jumps in about 4 nm nickel nanoparticles, assembled naturally into hexagonal closed packed (hcp) lattice; yet, magnetic susceptibilities in contrast reveal evolution of QSEs with decrease in particle size. Nickel nanoparticles we studied here were their compacted pellets of average particle sizes in the range ~ 4 - 10 nm prepared using trioctylphosphine (TOP) and oleylamine as surfactants and nickel acetylacetonate as precursor of Ni nanoparticles.

2. Theories of Heat Capacity

To begin with, we have analyzed our data using several contributions to the heat capacity with a few phenomenological parameters. Now, in a free-electron model for the bulk metal

the Fermi energy (EF) is independent of the particle size. Conversely, in smaller particle size, there are fewer conduction electrons (N) so that the filled electronic states at zero temperature (T = 0) is smaller. However, since all states are filled up to EF, which is fixed, then the energy level spacing G between the states increases with decrease in particle volume V [Halperin 1986]

$$\delta = \frac{4E_F}{3N} \propto V^{-1} \text{ or } d^{-3} \quad (1)$$

for spherical particle. Even though the particle size of 14 nm for silver for example with $\delta/k_B \sim 1K$ is easily accessible experimentally, it is not yet established clearly [Halperin 1988]. Moreover, the specific heat of a metal particle would be linear similar to that of the bulk metal for $k_BT >> \delta$ but switch to an exponential dependence at low temperatures (for $k_BT >> \delta$)[Kubo 1962].

$$C(T) = k_B exp\left(\frac{-\delta}{k_BT}\right), \text{ for } T \rightarrow 0. \quad (2)$$

However, it is impossible to perform such experiments on a single particle. Experimentally feasible samples in earlier studies contain large number of particles with varying sizes and shapes. This leads equation (2) to a simple integral power law, and translates into the fact that despite its simplicity and very fundamental nature, no clear experimental observation on the quantum size effect has yet been reported in the last five decades since its prediction [Kubo 1962]. In fact, in equation (2), all levels are assumed to be equidistant and hence expected to be difficult in its experimental verifications. However, in the advent of NLs, observations of what are predicted in equation (1) and equation (2) experimentally may not be null.

In view of the above, the heat capacity of such a compacted NL sample may then be represented approximately by [Halperin 1986]

$$C(T) = \gamma T + A_n T^2 + \beta T^3 + A_0 Exp\left(\frac{-B}{T}\right). \quad (3)$$

Here, $\gamma = \pi^2 k_B^2 D(E_F)/3$ and $\beta = 12\pi^4 R/5\theta^3$ are due to conduction electrons and phonons, respectively. D(EF) is the density of states at the Fermi energy (E_F), k_B is the Boltzmann constant, R is the universal gas constant and T is the Debye temperature. The other contribution to heat capacity of interest is T2 term. It is presumed that the possible lower symmetry at the surface, the band structure on the surface layers could to be different from that of the bulk. Interestingly, electron interactions will be altered.

3. Heat Capacity Measurement Results

Figure 1 displays the temperature dependence of the representative heat capacity, CP(T), of 4 nm, 4 nm (R), 5.0 nm and 10.1 nm Ni nanoparticles and Ni bulk as reference: 4 nm (R) sample served the repetition of the measurements to check for reproducibility of the data of 4 nm sample when it was prepared under similar conditions, and similarly the other samples, to assess evolution of CP. Clearly, Cp of the NPs is larger than that of the bulk Ni. It is noted that while CP curves for smaller NPs are very close to each other, especially above 45 K for 4 nm, 4 nm (R) and 5.0 nm samples. However, CP for 10.1 nm NPs is quite distinct from those of other samples. It tends to, yet well above, that of the bulk. They in general indicate change in the electronic and phonon contribution to the heat capacity. There is, in overall, enhancement of CP at 120 K as the particle size decreases. The values are at slight random variation with smaller sizes, indicating that the particle sizes are just an average but the actual size could be varied not only that the surface interactions with the surfactants and environment could be there during and after their preparations. They could drastically influence the final physical property under consideration say heat capacity.

The most dramatic observation is the exponentially decaying heat capacity CP of 4 nm NPs below about 45 K (Figure 5.1). It can be fitted as CP = 2336e-140(8)/T, expected for T→0 and for equal level spacing δ i.e. kBT<< δ, to the experimental CP data below 45 K (Figure 1, inset). This, that too setting in at 45 K, is remarkable since the level spacings here, as will be seen below, are unequal. This is so, in spite of the probable (i) splitting of the degeneracy of the energy levels due to the atomic irregularities on the surface and produce an average level spacing δ, and (ii) deviation (above 17 K) from the original odd-even regime (< 1 K) and hence with their possible wash out. The fitted parameter, δfit = 140(8) K, is significantly larger than those quantum jumps observed at and below 45 K (Figure 2). This is attributed to (i) the poor fitting (χ2 = 32) due to the quantum jumps (Figures 1 & 2) and or (ii) the probable existence of a dominant size of less than 2 nm in the background equivalent to δfit = 140(8) K, a little less than double the size determined from Scherrer formula [Okram et al. 2015], but looks consistent. On the contrary, null results are seen in other samples. They not only look to support, but also strengthen further the earlier null results. Hence, the exponentially decaying CP of 4 nm specimen above 17 K could be a chance that attains near to perfection meeting QSE at such a high temperature.

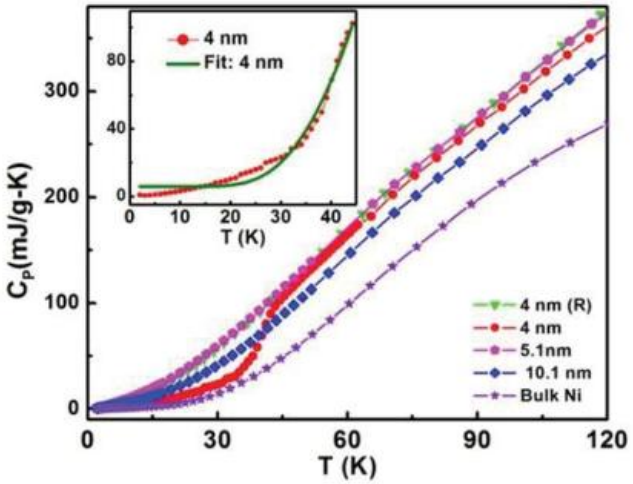

Figure 1: Heat capacity (CP) data. CP data of 4 nm, 4 nm (R), 6.0 nm and 10.1 nm natural nickel Nano lattice samples along with that of bulk nickel as reference. CP of 4 nm sample shows an exponential decay characteristic. Inset: Solid (olive) curve is the exponential decay fit CP = 2336e-140(8)/T to the experimental CP data of 4 nm sample (line + symbol).

In order to understand this better, Figure 2 represents excess heat capacity ΔCP of 4 nm NPs on the right side ordinate. Its derivative is shown on the left side ordinate. The distinct appearance of the quantum jump features is inferred from these plots. ΔCP exhibits abrupt jumps at 45.2 K, 40.2 K, 36.1 K, 32.1 K, 27.1 K, 22.1 K and 17.1 K, respectively. Moreover, the negative excess heat capacity CP appeared below 31 K and 34 K is consistent with earlier report on Na cluster.

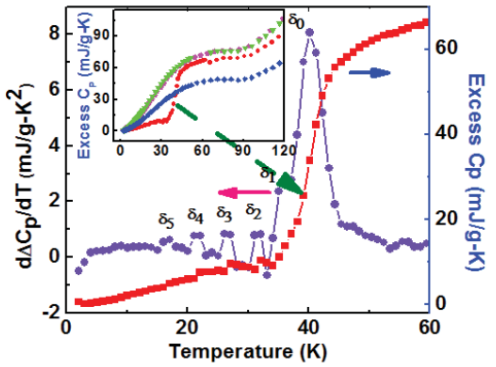

Figure 2: Quantum jumps in the excess heat capacity ΔCP and its derivative dCP/dT. ΔCP of 4 nm NPs (right ordinate) and its derivative (left ordinate). The abrupt quantum jumps in ΔCP are seen as peaks in dΔCP/dT. They are identified as various level spacings (see text). The inset depicts ΔCP of all the four Ni nanoparticle samples to distinguish the anomalous characteristics of 4 nm sample: 4 nm (red rectangle), 4 nm (R) (green triangle), 6.0 nm (pink pentagon) and 10.1 nm (blue vertical rectangle) samples.

These quantum jumps are seen as peaks in the dΔCP/dT plot and reflect presence of different Kubo energy spacing's. They are denoted as δ_0, δ1, δ2, δ3, δ4 and δ5. Their respective differences have been defined as Δδ1 = δ1 - δ0, Δδ2 = δ2 - δ1, etc., such that Δδ1 = 4.1 K, Δδ2 = 4.0 K, Δδ3 = 5.0 K, Δδ4 = 5.0 K, Δδ2 = 5.0 K, respectively. They are clearly distinct and some of them even have equal values. The various quantum jumps and unequal jump widths (Δδ's) are expected for practical MNPs.They appear to indicate the discrete nature of set of NPs that possess such level spacings that differ from their smaller or bigger NPs nearly exactly the number of electrons available in each set of these nanoparticles. This is suggestively combined with other ensembles, which have decreasing energy levels and hence corresponding quantum jumps (Figure 3) since particles may have distributed level spacings even for the same estimated size. They therefore may indicate partially the question of whether there are randomly distributed electronic level spacings over the sample or not. These distinct features are however absent in other Ni nanoparticle samples Figure 4, but consistent with the restrictive nature of quantum size effects, $k_BT<<\delta$, for all particle sizes studied thus far.

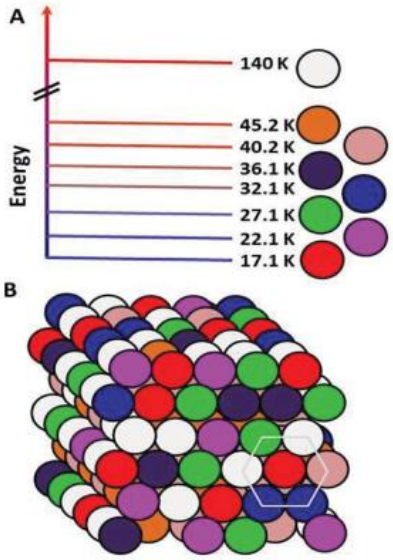

Figure 3: Scheme 1 Energy levels in 4 nm hexagonally closed packed, hcp, nickel particle specimen with faced centered cubic atomic structure inside each of them. A, Energy levels due to various sub-ensembles of nanoparticles represented by white, orange, light red, purple, blue, green, pearl magenta and red color spherical particles responsible for exhibition of exponential heat capacity behavior, quantum jumps at 45.2 K, 40.2 K, 36.1 K, 32.1 K, 27.1 K, 22.1 K and 17.1 K, respectively, in the specimen. B, The hcp specimen with different sizes/ types of particles. Particles are shown as of the same size from the point of view of hcp structure formation. However, their response to the heat capacity is different in size based on the transformation properties of the Hamiltonian that is decided by the symmetry, actual size and interaction with their immediate neighborhoods [Halperin 1986].

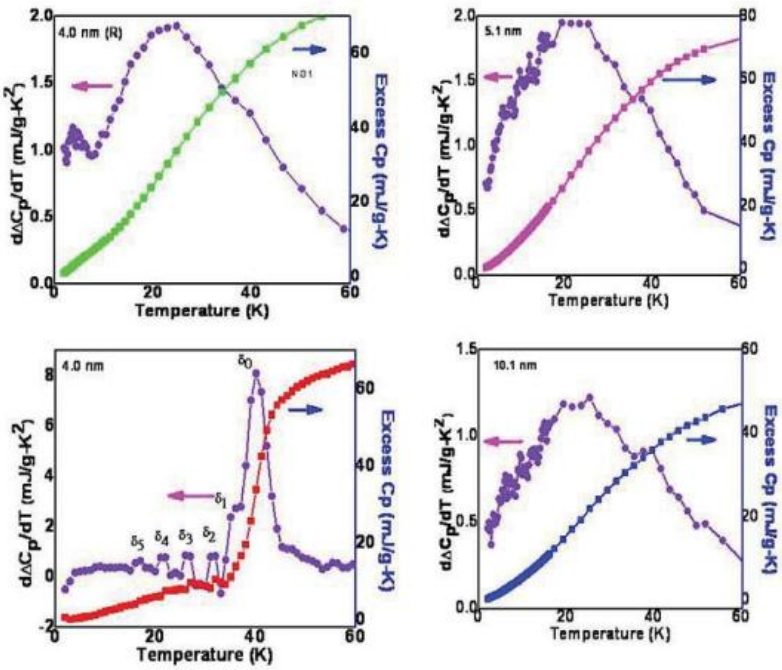

Figure 4: Quantum jumps in the excess heat capacity ΔCP and its derivative dCP/dT. ΔCP of 4 nm NPs (right ordinate) and its derivative (left ordinate). The abrupt quantum jumps in ΔCP are seen as peaks in dΔCP/dT. They are identified as various level spacings. Similar plots are shown for 4 nm (R), 5.1 nm and 10.1 nm samples. Note their features of dΔCP/dT without any clear peaks even the one near 5 K in 4 nm (R) sample. Only 4 nm sample exhibits clear quantum size effect.

4. Magnetization Study

Magnetization can be a powerful technique to study possible identification of structural phases in a multiphasic material for which the magnetization characteristics are different. This is applied in mixture of hcp and fcc structures of 8.5 nm and 18 nm Ni nanoparticles, leading to exhibition of two distinct zero-field cooled (ZFC) magnetization peaks due to the superparamagnetic blocking (TB) at 12 K and 220 K, respectively. They are further corroborated with ZFC magnetization peak at ~ 12 K of pure hcp Ni of 12.9 nm and above 300 K of pure fcc Ni of ~30nm [Chen et al. 2007, Singh et al. 2016a]. Considering that these situations are applicable in the present samples, we assign double peaks in ZFC magnetization data at 5 K and 200.9 K of 3.8 nm sample, 3.2 K and 117.4 K of 4 nm sample, less than 2 K and 81.9 K of 6.0 nm sample due to the presence of hcp and fcc phases in these smaller particle size samples.

Note the systematic reduction of TB of hcp phase as the particle size increases from 3.8 nm to 6.0 nm through 4.0 nm. The relatively lower TB in the present samples, compared to those of distinct mixture of two phases or only hcp phase, is tentatively attributed to close proximity interaction with fcc phase and or related to the much smaller particle size for hcp phase in the naturally coexisting core-shell structure. In the larger particle size samples, only a single peak each in ZFC data is apparent supporting the finding from XRD analysis of pure fcc phase. Moreover, FC curves exhibit systematic change in the magnetic behaviors with increase in particle size. Thus, it is concluded that hcp and fcc phases coexist for particles with average size up to 6.0 nm beyond which only pure fcc phase triumphs.

In order to understand better the magnetic properties of these nanoparticles, magnetization (M) as a function of magnetic field (H) was carried out at 3 K and 300 K. M-H loops is invisible for 3.8 nm samples at 300 K, while all others show M-H loops. They are indicative of ferromagnetic state at 300 K. Ferromagnetic state is attributed to the surface spin states that are normally found in nanoparticles since TB for fcc phase exists well below 300 K.

M-H loops are seen (Figure 5.8) however at 3 K for all the samples indicating that they are ferromagnetic at this temperature justifying super paramagnetic states above TB consistent with earlier reports on other nanoparticles. Both the HC's for 300 K and 3 K show decreasing trends as the particle size increases up to 6.0 nm. Beyond this, a sudden rise and then very slow increase for 3 K but a slight decrease for 300 K occurs.

5. Thermoelectric Power Measurement

The systematic variations of thermo power (S) with TOP concentration were observed shown if Figure 5. This reflects the strong influence of particle size on the thermo power of Ni-Nps. The signs of S are all positive indicating that holes are the majority carriers in these NPs, in contrast to the negative sign of their bulk counterpart, that infect further strengthen earlier reports. There is also a remarkably significant increase of S at 300K, while it increases nearly exponentially as temperature drops further. Such remarkable features in S are understood to be due to rampant grain boundary scattering of charge carriers and quantum confinements in these nanoparticles.

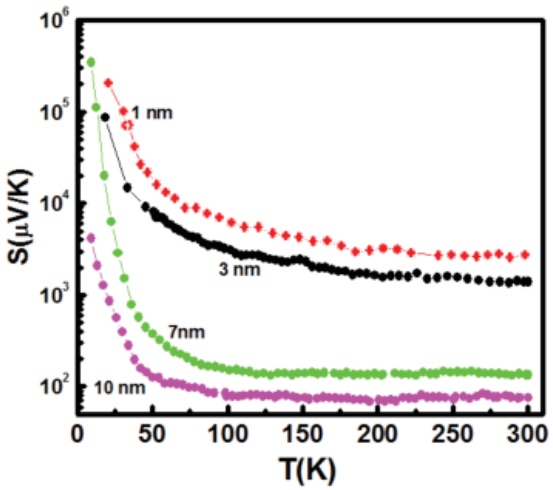

Figure 5: Variation of thermo electric power with particle size

The significantly large value of S in the range 10^3 to 2×10^5 μV/K at T = 20 K , much higher than that reported earlier in larger particle size is clearly suggestive of low temperature thermoelectric application potentials of these Nano lattices.

6. Nano Lattice Formation Through SAXS, XRD And TEM

A important method for defining the nanolattic structures is the small angle X-ray dispersal. Figure 6 shows these details for the nickel nanoparticles in oleylamine and trioctyl phosphine of different particle sizes (~4 to 10 nm) with no external surfactants, reagents or outside forces. The lattice flats formed by mono-dispersed nanoparticles are assigned several low angular peaks clearly seen in the SAXS results. Since there are no external force forces for preparing them, the naturally occurring structure of nano lathes is symbolic, since the latter is due to the atomic facial based cubiic (fcc) grid distinctive from wide angled x-ray diffraction. The chosen field of electrical diffraction patterns of the electron beam perpendicular to the TEM plane for the 10 ml electrons (Figure 6a, left bottom inset) and parallel to the plane of the TEM grid line for the 10 ml sample (Figure 6a). The TEM image of the hexagonal arrangement with seven nanoparticles almost spheric in shape is shown in Figure 6a, in the lower right inset.

To ensure that the peaks in Figure 6b, c and d are due to self- assembly of bulk 3D hcp structures of nanoparticles, analytical calculations were made using these peaks. For this, $\sin^2\theta$ values were determined from

$$\sin^2\theta=A(h^2+kk+k^2)+Cl^2$$

Where $A=\lambda^2/3a^2$, $C=\lambda^2/4c^2$, λ is the wavelength of the -ray and other parameters have their usual meanings. Permissible values of (h2 +hk+k2) being 1, 3, 4, 7, 9, etc for hcp structure, the observed $\sin^2\theta$ values were divided by 1, 3, 4, etc.

These numbers were examined to find out that any of the quotients (nearly) match the observed $\sin^2\theta$ and hence the tentative value of A was determined. The correspondingly matched values of (hk0) were chosen as the expected (hk0) values. Using these (hk0), and A (h2 +hk+k2) values, value of C is determined from equation such that Cl^2 is in the ratio of 1, 4, 9, 16, etc. This procedure readily enables to identify the

peaks in the pattern systematically. Final check was done by a comparison of observed and calculated $\sin^2\theta$ values.

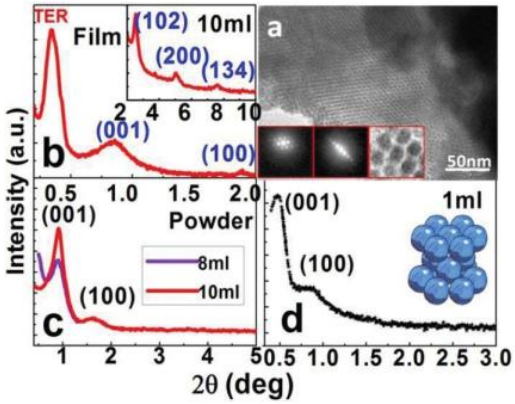

Figure 6: Transmission electron microscopy (TEM) images and SAXS patterns of Ni nanoparticles. (a) Representative TEM image of 10ml sample nanoparticles. Inset: SAED of hexagonally arranged self-assembled Ni Nano lattice when the electron beam is perpendicular (left) and parallel (middle) to the plane of copper grid, and magnified portion of seven (hexagonally arranged) nanoparticles (right). (b) SAXS of glass-drop-casted film of 10ml sample with higher angle in inset. The analytically calculated (hkl) values for hcp phase are given; total external reflection (TER) is due to glass substrate. (c) Powder SAXS for 10ml and 8ml Ni bulk nanoparticle samples. (d) Powder SAXS of 1ml Ni bulk nanoparticle sample. Inset: an illustration of hexagonal closed-packed unit cell representing the nanoparticle unit cell.

The SAXS peaks of the samples 10ml can therefore be routinely compared with (hkl) bulk values of 3D hcp nano lattice (Figure 6b), a=3.812 nm, c=7.131 nm and c / a=1.87. As the total external reflection of the glass substratum in Figure 3.2, the top near 2 pit = 0.36 ° was established. Instead our attempts were always different from the observed for finding the peak positions in their probable fcc Nano grids using the average particle size of 4.0 nm. It shows that the SAXS peaks observed are due to the bulk 3D hcp nano grid rather than the fccnano grid. Hcp nano-glazing has been defined as the peaks of other samples. The samples in 10ml and 8ml reveal hexagonal structures of 4,39 nm & 4,4 nm, 7,41 nm & 7,45 nm & 1,67&1,69 in powder shapes (Figure 6c) respectively. The nanolatite parameters are somewhat larger for the 10ml powder sample than the thin film parameters. The 1ml powder sample nano mesh parameter is a=8.09 nm, c=13.28 nm with c / a=1.64. (see Figures 3.1d). Even in powder form, these natural hcp Nano lattices are striking.

7. Conclusion

The special properties of metal nanoparticles and their potential use in various fields such as microelectronics, optoelectronics, catalysis, photocatalytics, magnetic materials, storage of information, have attracted considerable interest in recent years. In particular, magnetic nanopartics can be used in ultra-high magnetic storages, ferrofluids, magnetic cooling systems, magnetic resonance imaging contrast agent, magnetic drug delivery carriers, catalysis, and a number of new phänomens resulting from their mutual interactions. However, because of their use in many practical applications, such as magnetic materials, material conduction and catalysts nickel nanoparticles have gained significant attention. The size and shape of these nanoparticles (NPs) depend on the majority of physical and chemical properties. In order to obtain nanoparticles with a controlled mean size and a restricted distribution in size, the production of synthetic roads is important. It is appropriate. Synthetic protocols are needed, in which a substantial monitoring over certain parameters can be applied to optimize the new properties that are often influenced by the particle size, shape and crystalline phase. Several different physical and chemical methods have been employed in the production of metal nanoparticles, such as metal evaporation-condensation, electrochemical methods, sonochemical synthesis, salt reduction and organometal neutral degradation of precursors. Chemical syntheses are usually simple and cost-effective in contrast to physical approaches.

The nano lattice formability is explained based on the balanced attractive and repulsive energies of cation–anion pairs of the dissociated surfactant molecules or impurities. In particular, natural nano lattice is formed when nonionic long- and triple-chained TOP is used as surfactant, but not with that of long-chain (OA) or phenyl group (TPP) surfactants. This nano lattice formation was tentatively understood qualitatively in two ways. First, a head of surfactant (P or TOP) binds on the surface of Ni particle while organic tail in turn binds tail of another surfactant such that particles are glued at a fixed distance. When the number of such processes increases, nano lattice formation takes place with the minimization of the total surface energy. Secondly, according to zeta potential, FTIR and XPS data, cations of the ion pairs of the dissociated surfactant molecules or impurities attached on a nanoparticle may attract the anions of the surrounding nanoparticles until they sense the presence of other cations of the latter, leading to repulsion. Detailed analysis of X-ray diffraction (XRD), synchrotron radiation X-ray absorption fine structure (EXAFS) and magnetization data of mono dispersed nickel nanoparticles (NPs) of different sizes (3.8 nm to 10.1 nm) that exhibit natural nano lattices has been carried out. It has been demonstrated that particles of size in the range 3.8 nm to 6.0 nm have rather complex coexistent atomic hexagonal closed-packed and face-centered cubic crystal structures, and associated highly reduced coordination numbers, disturbed electronic structure, and surface atom coordination to the surfactants. They lead to complex magnetic properties of coexistent ferromagnetism and super paramagnetic. Trend is significantly different when the particle size is above 6.0 nm. They have been ascribed to dominant roles of the ligands of trioctylphosphine and oleylamine over the surface nickel atoms in forming covalent bonds and concomitant disturbance in the atomic lattices.Quantum size effect-induced exponentially decaying heat capacity, below 45.2 K, associated with quantum jumps, was observed exceptionally in 4 nm, naturally assembled hcp lattice of, nickel nanoparticles. In fact, quantum size effect-induced heat capacity of metal nanoparticles at low temperatures was predicted 79 years ago to be exponential and our results demonstrated conclusively the experimental observation.

References

1. [Gao et al. 2004] Y. Gao, Y. Bao, M. Beerman, A. Yasuhara, D. Shindo and K. Krishnan, Appl. Phys. Lett., 84, 3361 (2004).
2. [Gajbhiye et al. 2008] N. S. Gajbhiye, S. Sharma, A. K. Nigam and R. S. Ningthoujam, Chem. Phys. Lett., 466, 181 2008).
3. [Glatter&Katky 1982] O. Glatter and O Katky, Small angle X-ray Scattering, Academic Press, Newyork (1982).
4. [Gleiter et al. 1982] H. Gleiter, Mat. Sci. Engg. 52, 91 (1982).
5. [Gleiter2000]H.Gleiter, Acta. Mater. 48, 1 (2000).
6. [Gorkov&Eliasberg 1965] L. P. Gorkov& G. M. Eliasberg, Sov. Phys. JETP 21, 940 (1965).
7. [Gopidas et al. 2003] K. R. Gopidas, J. K. Whitesell, M. A. Fox, Nano Lett., 3, 1757 (2003).

8. [Guinier&Fournet 1975] A. Guinier and G. Fournet, Small angle Scattering of Xray, John Wiley and Sons, New York, (1975).
9. [Halperin 1986] W. P. Halperin, Rev. Mod. Phys. 58, 533 (1986).
10. [Hart et al. 2013] J. N. Hart, P. W. Maya, N. L. Allana, K. R. Hallamb, F. Claeyssens, G. M. Fugea, M. Rudaa and P. J. Heard, J. Solid State Chem., 198, 466 (2013).
11. [Haubold et al.1989] T. Haubold, R. Birringer, B. Lengeler, H. Gleiter, Phys. Lett. A.135, 461 (1989).
12. [Haubold et al. 1991] T. Haubold, W. Krauss and H. Gleiter, Phil. Mag, Lett., 63, 245 (1991).
13. [Hodes et al. 1987] G. Hodes, A. A. Yaron, F. Decker and P. Motisuke, Phys. Rev.B 36, 2415 (1987).
14. [Hou et al. 2005] Y. Hou, H. Kondoh, T.Ohta and S. Gao, Appl. Surf. Sci. 241, 218 (2005).
15. [Huebner 1964] R. P. Huebner, Phys. Rev. 136, A1740 (1964).
16. [Hu et al. 2002] W. K. Hu, X. P. Gao, M. M. Geng, Z. X. Gong, D. Noreus, J. Phys. Chem. B 109, 5392 (2005).
17. [Huebner 1965] R. P. Huebner, Phys. Rev. 140, A1834 (1965). [Hufner et al. 1996] S. Hufner, Springer-Verlag, Berlin 82 (1996).
18. [Hyeon et al. 2001] T. Hyeon, S. S. Lee, J. Park, Y. Chung and H. B. Na, J. Chem. Soc., 123, 12798 (2001).
19. [Iterrante& Smith 1998] L.V. Iterrante and M.J.H. Smith, Chemistry of advanced materials, WILEY-VCH (1998).
20. [Jaiswal et al. 2016] A. Jaiswal, S. Gaherwal, P. D. Lodhi, J. Singh, N. Kaurav and M. M. P. Shrivastava, AIP Conf. Proc. 1728, 020435.

